

## Donor–Acceptor Systems

# Symmetry Effects in Photoinduced Electron Transfer in Chlorin–Quinone Dyads: Adiabatic Suppression in the Marcus Inverted Region

Yvonne Abel,<sup>[a]</sup> Ivan Vlasiouk,<sup>[b]</sup> Enno Lork,<sup>[c]</sup> Sergei Smirnov,<sup>\*,[d]</sup> Marat R. Talipov,<sup>\*,[d]</sup> and Franz-Peter Montforts<sup>\*,[a]</sup>

*Dedicated to Professor Albert Eschenmoser on occasion of his 95th birthday*

**Abstract:** In donor–acceptor dyads undergoing photoinduced electron transfer (PET), a direction or pathway for electron movement is usually dictated by the redox properties and the separation distance between the donor and acceptor subunits, while the effect of symmetry is less recognized. We have designed and synthesized two isomeric donor–acceptor assemblies in which electronic coupling between donor and acceptor is altered by the orbital symmetry control with the reorganization energy and charge transfer

exothermicity being kept unchanged. Analysis of the optical absorption and luminescence spectra, supported by the DFT and TD-DFT calculations, showed that PET in these assemblies corresponds to the Marcus inverted region (MIR) and has larger rate for isomer with weaker electronic coupling. This surprising observation provides the first experimental evidence for theoretically predicted adiabatic suppression of PET in MIR, which unambiguously controlled solely by symmetry.

## Introduction

Numerous dyads consisting of covalently linked porphyrinoid donors and quinone or fullerene acceptor moieties were investigated as model systems to understand light induced electron transfer of photosynthesis and to design efficient artificial photosynthesis systems.<sup>[1–11]</sup> The studies showed that the redox properties of the donor and acceptor units and their relative separation and orientation dictate the efficiency of light induced charge separation in these model systems.<sup>[12–20]</sup> Less no-

ticeable, but recognizable in some cases, is the effect of symmetry,<sup>[21–28]</sup> that is the effect of the parity correlation of the donor/acceptor frontier orbitals,<sup>[21, 24–26, 29, 30]</sup> as well as appropriate spacer (bridge) orientation.<sup>[27, 28]</sup>

According to the Marcus theory of nonadiabatic electron transfer,<sup>[31–35]</sup> the rate constant of charge transfer from a donor, D, to an acceptor, A, can be calculated by Equation (1):

$$k_{A \leftarrow D} = (2\pi/h^2) |T_{AD}|^2 FC \quad (1)$$

where FC is the sum of thermally weighted Franck–Condon factors for nuclear coordinates of the reactants and the surrounding medium. The distance and the orientation dependencies of the rate constant are primarily described in the coupling matrix element,  $T_{AD}$ , which is approximately proportional to the overlap integral between the wave functions of the donor,  $\psi_D$ , and the acceptor,  $\psi_A$  [Eq. (2)].<sup>[32–35]</sup>

$$T_{AD} \propto S_{AD} = \langle \psi_A | \psi_D \rangle \quad (2)$$

One can therefore relate the overlap between the donor–acceptor LUMOs as being responsible for the photoinduced electron transfer (PET) when the electron donor is excited.

In this paper, we use two types of chlorin (donor)–naphthoquinone (acceptor) dyads, shown in Figure 1, to demonstrate the importance of the parity correlation in the donor/acceptor LUMOs to PET. Quite a few examples of dyads with chlorophyll donors have been reported, while the predominant number of investigated dyads make use of porphyrin donors.<sup>[36–43]</sup> The high symmetry ( $D_{4h}$ ) of the porphyrin system A in Figure 1

[a] Dr. Y. Abel, Prof. Dr. F.-P. Montforts

Institut für Organische und Analytische Chemie  
FB2, Universität Bremen, Leobener Straße NW2/C, 28359 Bremen (Germany)  
E-mail: mont@uni-bremen.de

[b] Dr. I. Vlasiouk


Oak Ridge National Laboratory, Oak Ridge, Tennessee 37831 (USA)


[c] Dr. E. Lork

Institut für Anorganische Chemie und Kristallographie  
FB2, Universität Bremen, Leobener Straße NW2/C, 28359 Bremen (Germany)

[d] Prof. Dr. S. Smirnov, Prof. Dr. M. R. Talipov

Department of Chemistry and Biochemistry  
New Mexico State University, Las Cruces, New Mexico 88003 (USA)  
E-mail: sns@nmsu.edu  
talipovm@nmsu.edu

 Supporting information and the ORCID identification number(s) for the author(s) of this article can be found under:  
<https://doi.org/10.1002/chem.202002736>.

 © 2020 The Authors. Published by Wiley-VCH GmbH. This is an open access article under the terms of Creative Commons Attribution NonCommercial-NoDerivs License, which permits use and distribution in any medium, provided the original work is properly cited, the use is non-commercial and no modifications or adaptations are made.

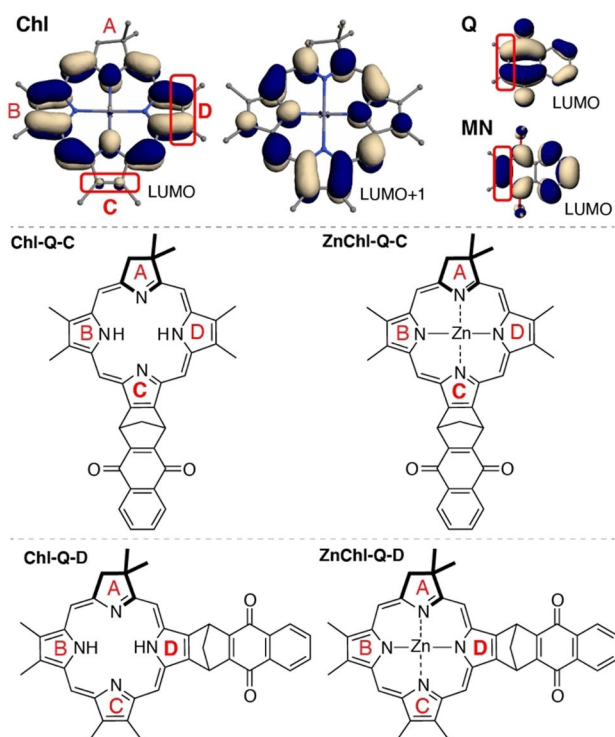


**Figure 1.** Top: LUMOs of chlorin (Chl), 1,4-naphthoquinone (Q) and 1,4-dimethoxynaphthalene (MN). LUMOs of ZnChl have similar shape (not shown). Middle and bottom: Chl-Q isomeric assemblies with norbornadiene bridge Chl-Q-C **8** (middle) and Chl-Q-D **5** (bottom) and their Zn-chlorin analogues.

coins its absorption properties and does not allow for a convenient observation of the symmetry effect on PET (Figure 2).

In contrast to porphyrin (Figure 2A), chlorin type chromophores (Figure 2C), present in naturally occurring chlorophylls of plant photosynthesis show a lower  $C_{2h}$  symmetry (Figure 2B). The reduced symmetry of chlorin gives rise to different light absorbance most noticeable by the green color of chlorophylls compared to the red of porphyrins for example, red blood pigment heme. The different absorption properties of both systems, porphyrin and chlorin, can be interpreted in terms of MO theory.<sup>[44–47]</sup> While porphyrin has degenerate LUMO orbitals of  $e_g$  symmetry,<sup>[48]</sup> the chlorin molecule has the degeneracy of LUMO lifted due to the aliphatic saturation of one pyrrole ring (Figure 1). The saturated pyrrole lacks the two  $\pi$  electrons necessary for exciting a corresponding  $e_g$  MO (say

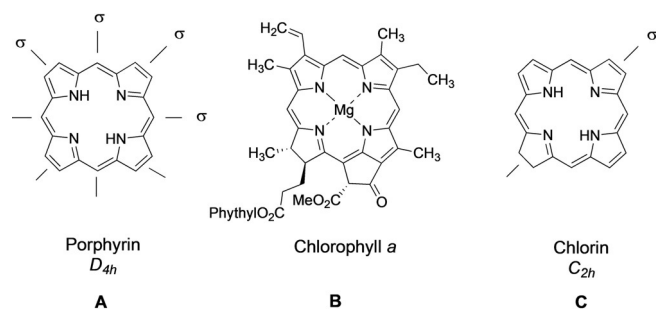


**Figure 2.** Symmetry of porphyrin versus chlorin the chromophore of chlorophyll a.

$e_{gx}$ ), thus raising its energy and leaving a transition to another MO,  $e_{gy}$ , almost exclusively responsible for the lowest energy excited state. Such induced geometrical disproportionation can be used for funneling electron transfer along one preferential direction, which would be different in the two isomers that have the same acceptor molecule attached to different pyrrole rings. Due to the reduced symmetry in the case of chlorin, its effect on PET should become observable. In order to investigate this influence of symmetry we designed and synthesized appropriate chlorin naphthoquinone dyads **5** and **8** of different symmetry. Naphthoquinone has the parity of its LUMO appropriate for the maximum overlap with the LUMO of chlorin when linked to the pyrrole D (i.e. Chl-Q-D **5**, Figure 1), and minimum overlap when linked to the pyrrole C. Therefore, Chl-Q-D (**5**) is expected to have an improved coupling as compared with Chl-Q-C (**8**). Marcus theory [Eq. (1)] suggests that the two isomers, like in our case, with “identical” energies of the involved states but different  $T_{AD}$  should have the rates of charge transfer differ proportional to  $T_{AD}^2$ . Our system offers a good opportunity to test such prediction.

Accordingly, this work focuses on synthesis and photochemical studies of donor–acceptor assemblies Chl-Q-D (**5**) and Chl-Q-C (**8**). Opposite to a simplistic prediction, we found that PET transfer was dampened in the isomer with higher electronic coupling between donor and acceptor. This counterintuitive observation was connected to the realization that PET between Chl-Q-D and Chl-Q-C corresponds to the Marcus inverted region. Interestingly, several earlier theoretical works predicted such an effect of adiabatic suppression of PET arising due to the increased electronic coupling. To our knowledge, this report is the first experimental evidence to the nontrivial phenomenon of adiabatic suppression of PET. The details of this combined synthetic, spectroscopic, and computational work are described below.

## Results and Discussion

For construction of chlorin target structures Chl-Q-D (**5**) and Chl-Q-C (**8**) a general synthesis concept from the Bremen laboratory successfully applied for syntheses of several porphyrinoid and corrinoid macrocyclics was applied here.<sup>[49–56]</sup> The concept employs different monocyclic building blocks for each of the target chlorins **5** and **8** of different symmetry (Figure 3).

Pyrrolic building blocks 1–4 should be assembled together to form macrocyclic **5**. Constitutionally isomeric chlorin **8** should be obtained from pyrrole precursors 1, 2, 6 and 7 (Figure 3). Both target chlorins **5** and **8** exhibit  $C_1$  symmetry due to methyl substituents at saturated pyrrole rings A. But considering only the chromophores including naphthoquinone moieties the envisaged different (pseudo)symmetries of  $C_s$  for **5** and  $C_{2h}$  for **8** can be recognized. Key building blocks for divergent constructions of isomeric chlorins **5** and **8** are pyrroles **3** and **7** bearing required naphthoquinone moieties and appropriate functionalities in  $\alpha$ -positions. These functionalities allow linkage with adjacent ring units. Starting point for preparation of the different C and D pyrroles for chlorins **5** and **8** is pyrrole **9** which was achieved according a general synthetic procedure

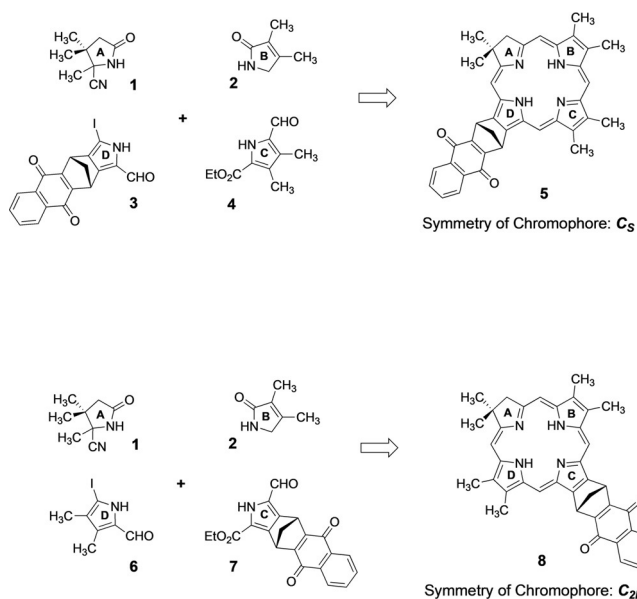
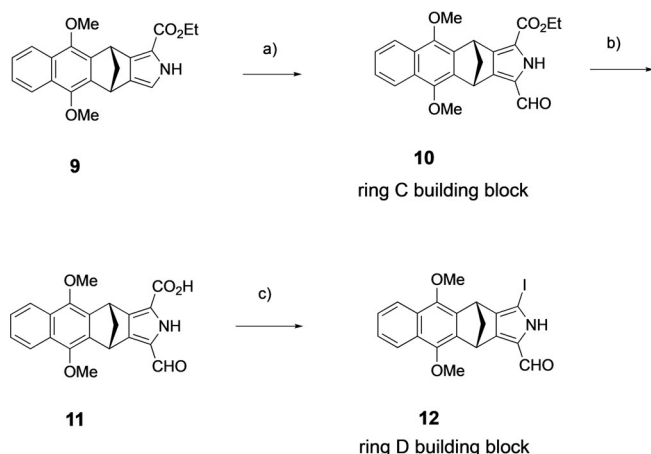


**Figure 3.** General synthesis concepts for construction of naphthoquinone chlorin dyads **5** and **8** of different symmetry.

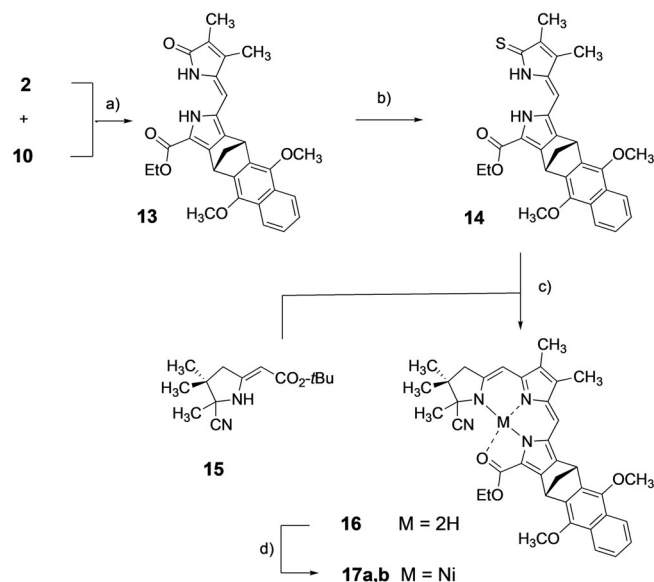


**Scheme 1.** (a)  $\text{POCl}_3$ , DMF,  $\text{ClCH}_2\text{CH}_2\text{Cl}$ ,  $5^\circ\text{C}$  to reflux, 2 h, then NaOAc, reflux, 15 min (71%). (b) LiOH,  $\text{H}_2\text{O}$ , THF,  $102^\circ\text{C}$ , 1.5 h (100%). (c) (i)  $\text{NaHCO}_3$ ,  $\text{H}_2\text{O}$ , 15 min,  $73^\circ\text{C}$ ; (ii)  $\text{I}_2$ , KI,  $\text{H}_2\text{O}$ , ultrasonic bath,  $73^\circ\text{C}$ , 45 min (72.2%).

previously developed.<sup>[57,58]</sup> Vilsmeier formylation of **9** directly afforded aldehyde **10** as ring C building block for chlorin **8**. Subsequent hydrolysis of ethyl ester in **10** followed by iodination of intermediate carboxylic acid **11** yielded pyrrole ring D precursor for chlorin **5** (Scheme 1). Hydronaphthoquinone dimethyl ether moiety of starting pyrrole **9** instead of the final quinone structure is a consequence of requirements in the course of preparation of pyrrole **9**.<sup>[58]</sup> The hydronaphthoquinone ether moieties can be transformed in later stages of chlorin syntheses into required quinone parts.

### Synthesis of naphthoquinone chlorin **8**

Base-induced condensation of ring B pyrrolinone **2** and ring C aldehyde **10** yielded BC dipyrromethenone intermediate **13** in almost quantitative yield (Scheme 2). Very strong Schwesing-

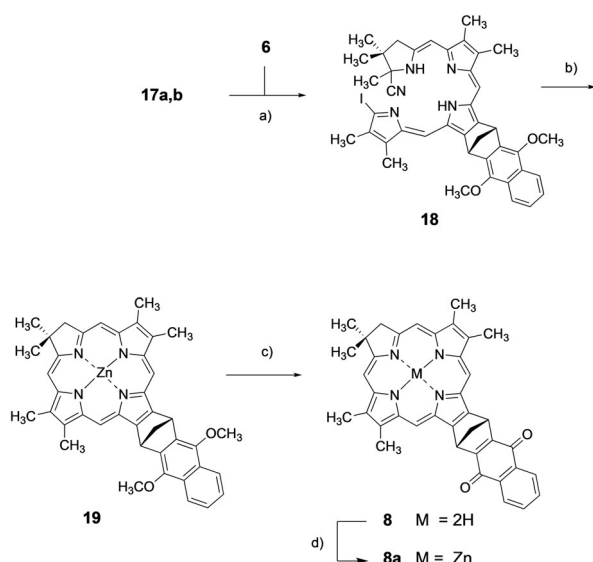


**Scheme 2.** (a) 2-*tert*-Butylimino-2-diethylamino-1,3-dimethyl-1,3-diaza-2 $\lambda^3$ -phosphacyclohexane (BEMP), benzene, reflux, 14 h (93.7%). (b)  $\text{P}_4\text{S}_{10}$ ,  $\text{NaHCO}_3$ , THF, Ar, room temp., 50 min, then add. of **13**, reflux, 3 h (78.3%). (c) (i) **15**, NBS,  $\text{CH}_2\text{Cl}_2$ , room temp., 20 min; (ii) **15-Br**, + **14**, DBU, MeCN, room temp., Ar, 40 min, alox chromatography; (iii) TFA, benzene,  $\text{P}(\text{CH}_2\text{CH}_2\text{CN})_3$ , alox chromatography. (d)  $\text{Ni}(\text{OAc})_2 \times 4\text{H}_2\text{O}$ , NaOAc,  $\text{CH}_2\text{Cl}_2$ , MeOH, Ar, room temp., 20 min (71.3% rel **14**).

er's base (BEMP) and azeotropic removal of water with benzene as solvent is crucial for success of the reaction.<sup>[52]</sup> Dipyrromethenone **13** was transformed into its thiolactam derivative **14** for preparing its linkage with ring A building block **15** by sulfide contraction.<sup>[50,51,53,59–61]</sup> The reaction sequence is initiated by bromination of enaminoide double bond of **15** and proceeded with high yield. Nucleophilic substitution of bromide of **15-Br** via its imino tautomer by thiolactam **14** formed a sulfur linked tricyclic thioiminoester. The thioiminoester underwent the actual intramolecular C–C bond formation by sulfide contraction with trifluoroacetic acid in the presence of thiophilic *tris*-cyanoethylphosphine in benzene. Ester cleavage and decarboxylation initiated sulfide contraction whereby benzene as solvent was crucial for success of the process as investigated and discussed in earlier studies.<sup>[53]</sup>

Because electron rich ABC tricycle **16** is quite sensitive to oxygen and light it was stabilized by complexation with nickel(II). Crystalline nickel complex **17a,b** proved to be very stable and occurred as binary mixture of diastereomers **17a** and **17b** due to chiral centers in position 20 of ring A and *nor*-bornane structure at ring C. For analytical purposes diastereomers were separated by HPLC [Polygosil 60-10,  $\text{CH}_2\text{Cl}_2/n$ -hexane (85:15)] and each single diastereomer was crystallized for X-ray structure investigations. These studies will be discussed later.

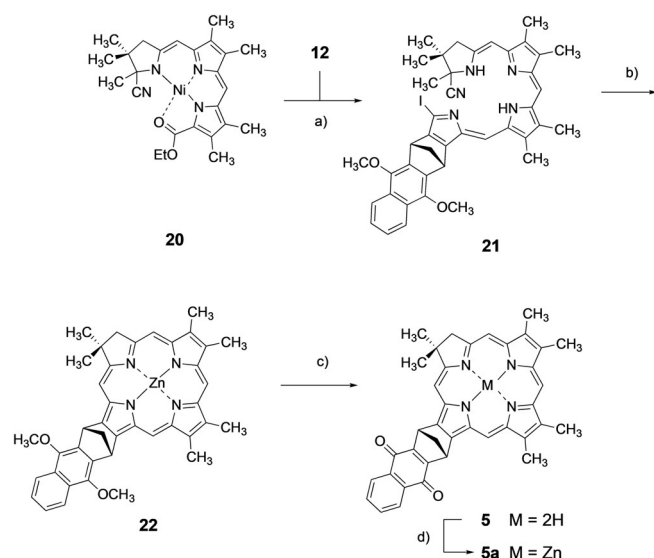
After hydrolysis of the ethylester function of **17a,b** the crude carboxylic acid undergoes direct acid induced condensation with decarboxylation and decomplexation with iodopyrrole aldehyde **6** to form tetrapyrrole **18** (Scheme 3). Crude metal-free tetracycle **18** was re-complexed with zinc(II) diacetate in situ under cyclization conditions. Heating of **18** with DBU in carefully degassed sulfolane afforded zinc chlorin **19**.



**Scheme 3.** (a) (i) **17a,b**, KOH (5 N), MeOH/H<sub>2</sub>O, (9:1), THF, reflux, 45 min; (ii) + **6** (2.5 equiv), CHCl<sub>3</sub>, *p*-TsOH, (0.4 N), reflux, Ar, 1 h; (iii) Zn(OAc)<sub>2</sub>, DBU, sulfolane (degassed), 80 °C, 2 h (22.3% rel. **17a,b**). (c) (i) BBr<sub>3</sub> (1 N in CH<sub>2</sub>Cl<sub>2</sub>), CH<sub>2</sub>Cl<sub>2</sub>, −78 °C to room temp., Ar, 12 h; (ii) + saturated NaHCO<sub>3</sub>, H<sub>2</sub>O, room temp., 1 h (32%). (d) Zn(OAc)<sub>2</sub>, NaOAc, MeOH, room temp., Ar, 20 min.

Zinc exercises a template effect for cyclization which is initiated by HCN elimination from ring A.

Enamine, formed by this elimination, undergoes nucleophilic attack at iodinated position of ring D to chlorin **19** via ring closure. Dimethylether of naphthoquinone moiety of chlorin **19** was cleaved under standard reaction conditions with BBr<sub>3</sub> at low temperature. The acidic reaction conditions also removed the central zinc(II) and oxygen from air lead to formation of the desired naphthoquinone moiety of target chlorin **8**. A small sample of **8a** for UV/Vis measurements was prepared according the procedure described for **5a** (Scheme 4).



**Scheme 4.** (a) (i) KOH (5 N), MeOH/H<sub>2</sub>O (9:1), THF, reflux, 45 min; (ii) + **12**, CHCl<sub>3</sub>, *p*-TsOH (0.4 N), reflux, Ar, 40 min (79%). (b) Zn(OAc)<sub>2</sub>, DBU, sulfolane (degassed), 80 °C, 2 h (36.2% rel. **20**). (c) (i) BBr<sub>3</sub> (1 N in CH<sub>2</sub>Cl<sub>2</sub>), CH<sub>2</sub>Cl<sub>2</sub>, −78 °C to room temp., Ar, 12 h; (ii) + H<sub>2</sub>O, room temp., 1 h (67.6%). (d) Zn(OAc)<sub>2</sub>, NaOAc, MeOH, room temp., Ar, 20 min (71%).

## Synthesis of naphthoquinone chlorin 5

Nickel tripyrrin **20** was applied for syntheses of several different chlorins and hexadehydro corrins is starting point for preparation of chlorin **5** here.<sup>[49,50,53]</sup> Tricyclic nickel complex **20** was linked with iodopyrrole aldehyde **12** (Scheme 4). Smooth hydrolysis of **20** to the free carboxylic acid and subsequent condensation with aldehyde **12** under decarboxylation yielded tetrapyrrole **21**.

Transformation of tetrapyrrole **21** into chlorin **22** was performed as for **19** in the presence of zinc(II) and DBU in sulfolane. Synthesis of target chlorin **5** was completed by cleavage of the naphthohydroquinone dimethylether with BBr<sub>3</sub> as described for isomeric chlorin **8**. Zinc(II) was also removed from the macrocycle under the acidic reaction conditions. To obtain zinc chlorin **5a** re-complexation with zinc(II) diacetate was performed.

## X-ray structures of nickel(II)tripyrin complexes **17a** and **17b**

Structural parameters gained from X-ray analysis revealed 1*RS*,8*SR*,20*SR* configuration for **17a** which was eluted first by HPLC (*t<sub>R</sub>* = 13.8 min). Less mobile HPLC fraction (*t<sub>R</sub>* = 17 min) **17b** exhibits 1*RS*,8*SR*,20*RS* configuration (Figure 4).

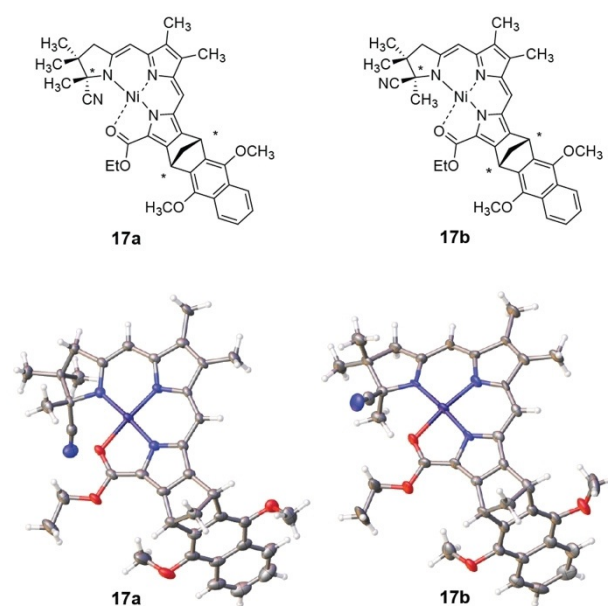


**Figure 4.** X-ray crystal-structure analysis of diastereomeric [ethyl-[(20-cyano-1,8,18,19,20,23-hexahydro-1,8-methano-2,7-dimethoxy-13,14,19,19,20-pentamethyl-21*H*-anthraceno[*b*]tripyrin)carboxylato]nickel(II)] (**17a** and **17b**; C<sub>38</sub>H<sub>38</sub>N<sub>4</sub>O<sub>4</sub>Ni, M 673,43, thermal ellipsoids showing at 50% level, **17a** solvent omitted for clarity). **17a**: Triclinic, space group P-1,  $\rho_{\text{calc}} = 1.328 \text{ Mg m}^{-3}$ ,  $Z = 2$ ,  $a = 1104.8$  (3),  $b = 1158.4$  (3),  $c = 1458.2$  (3) pm,  $\alpha = 84.38$  (2),  $\beta = 81.26$  (2),  $\gamma = 76.82$  (2)°,  $V = 1.7921$  (8) nm<sup>3</sup>,  $\mu(\text{MoK}\alpha) = 0.589 \text{ mm}^{-1}$ ,  $wR2 = 0.1392$ . **17b**: Orthorhombic, space group *Pbca*,  $\rho_{\text{calc}} = 1.363 \text{ Mg m}^{-3}$ ,  $Z = 8$ ,  $a = 1731.5$  (7),  $b = 1936.9$  (5),  $c = 1956.5$  (6) pm,  $\alpha = 90$  (2),  $\beta = 90$  (2),  $\gamma = 90$  (2)°,  $V = 6.562$  (4) nm<sup>3</sup>,  $\mu(\text{MoK}\alpha) = 0.639 \text{ mm}^{-1}$ ,  $wR2 = 0.1117$ .

Noteworthy for both diastereomers is the fact that carbonyl double bonds of ester functions exhibit remarkable long bond lengths of 127 pm. Based on CSD data retrieval including 2262 references for bond lengths of carbonyl groups of ethyl ester functions, an average bond length of 120.2 pm was reported,<sup>[62]</sup> while a retrieval for ethyl ester carbonyl fragments complexed by nickel(II) (15 references) indicated an average bond length of 122.6 pm. The maximum bond length among these references was reported as 125.4 pm. Stretching of the ester carbonyl bond of **17a** and **17b** by complexation with nickel(II) should facilitate ester hydrolysis. Indeed, this is an advantage for the next synthesis step with **17a,b**.<sup>[50–53]</sup> In both nickel complexes **17a** and **17b** coordinative Ni–N bonds have normal bond lengths between 182.5 and 187.2 pm, whereas Ni–O bonds are considerably longer, 193.4 pm. Planarity of all bonds directly involved in coordination around central nickel(II) is almost perfect. Average deviations from planarity of 7 pm for **17a** and 1 pm for **17b** are negligible.

### Spectroscopic characterization

The absorption spectra in Figure 5A show that the Q-band ( $\approx 600$ – $670$  nm) for the Chl-Q-D dyad (**5**) is much broader than those of chlorin itself and another isomer, Chl-Q-C (**8**). The

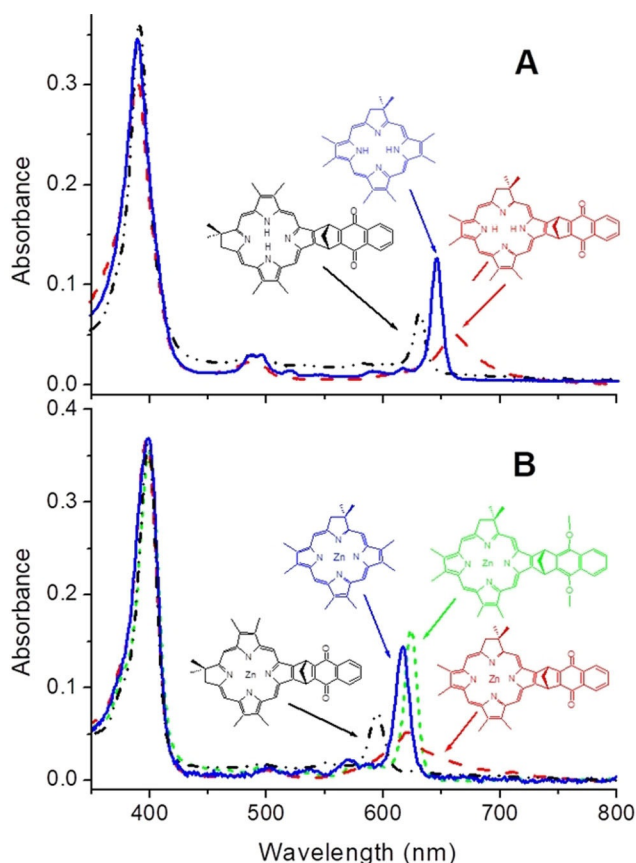


**Figure 5.** Absorption spectra of chlorin-based dyads in toluene: A) with free base chlorin, B) with Zn chlorin. Solid blue line denotes the spectra of Chl (A) and ZnChl (B), dashed red line-spectra of Chl-Q-D **5** (A) and ZnChl-Q-D **5a** (B), dashed black line-spectra of Chl-Q-C **8** (A) and ZnChl-Q-C **8a** (B), and dashed green line-spectrum of ZnChl-MN-D **15**.

effect persists with the Zn form of chlorins, as shown in Figure 5B. The increased width of the Q-band in ZnChl-Q-D (**5a**) and Chl-Q-D (**5**) dyads is due to the expected substantial charge transfer character in those transitions. The assignment is supported by the lack of such broadening in ZnChl-dimethoxynaphthalene-D (ZnChl-MN-D, **22**), see Figure 5B, in which electron-transfer character of the transition is suppressed owing to the electron-donating character of MN and mismatching parity of the chlorin/MN LUMOs (Figure 1).

Figure 6 shows that quinones in both isomers, C and D, do quench fluorescence of chlorin by means of charge transfer. Careful inspection of Figure 6 reveals that the residual fluorescence of the dyads has different spectra compared to those of chlorins, thus rejecting a possibility of trace amount of chlorins being responsible for the fluorescence. Since there is no charge transfer between MN and chlorin in ZnChl-D-MN (**22**), fluorescence of chlorin is not quenched in this dyad. Notably, fluorescence is quenched more efficiently for C isomers than for D isomers in both ZnChl-Q-C/ZnChl-Q-D (**8a/5a**) and Chl-Q-C/Chl-Q-D (**8/5**) pairs.

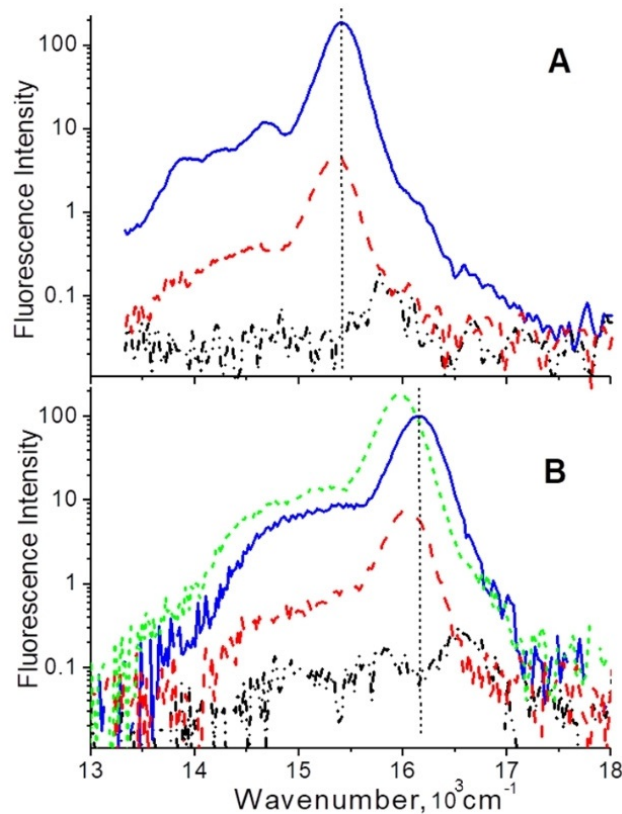


**Figure 6.** Normalized fluorescence spectra of the same dyads as in Figure 5.

### Theoretical modeling

It may seem surprising that fluorescence is quenched more efficiently in C than in D isomers of chlorin-quinone dyads despite the improved overlap and electronic coupling in D isomers and thus expected increase of the charge-transfer rate as per Equation (1). In the following discussion, we use DFT and

TD-DFT calculations to propose an explanation for this discrepancy. These calculations were undertaken at the B1LYP-40/6-31G(d)+PCM(toluene) level of theory, in which the standard BLYP functional was complemented by the 40% admixture of the exact exchange (i.e. Hartree–Fock) term to allow for the accurate description of the electronic structure of ion-radical and excited states.<sup>[63–67]</sup> Furthermore, we established that the 40% fraction of the Hartree–Fock term maximizes agreement with the experimental absorption spectra of the dyads presented in Figure 1, see Figure S2 in the Supporting Information.

The TD-DFT calculations, based on the ground state equilibrium geometries obtained using DFT approach,<sup>[41,68]</sup> revealed that the excited state  $S_1$  in both C and D isomers had mostly the charge-transfer (CT) character ( $D^+A^-$ ) as evidenced by the large values of their dipole moments,  $\mu(S_1)=29.6$  and  $25.9$  D, respectively (Figure 7). The excited state  $S_2$  had mostly the local excitation (LE) character ( $D^*A$ ) with  $\mu(S_2)=4.0$  and  $3.4$  D for C and D isomers, respectively (Figure 7). For comparison, the ground state dipole moments are  $\mu(S_0)=3.5$  and  $2.6$  D for Chl-Q-C (**8**) and Chl-Q-D (**5**), respectively. The dyads with Zn have similar values.

The electronic coupling between the CT and LE diabatic states, roughly estimated using the DFT calculations, was expectedly found to be larger in Chl-Q-D **5** ( $940\text{ cm}^{-1}$ ), see Figure S2 in the Supporting Information) than in Chl-Q-C isomer **8** ( $150\text{ cm}^{-1}$ ), in agreement with the qualitative analysis based on the LUMO orbital symmetries. Note that these large values are due to nonplanarity of norbornadiene bridge. Greater electronic coupling for the D isomers leads to the mixing of the CT and LE states and consequent increase of the oscillator strengths and decrease of the dipole moments in the  $S_1$  states of D isomers, as compared with C isomers, see Figure 7 and Tables S14–S17 in the Supporting Information. These findings from TD-DFT calculations are consistent with the experimental absorption spectra of the dyads, in which the CT feature is more pronounced in the case of Chl-Q-D **5** and ZnChl-Q-D **5a** (Figure 5). Similar trends were obtained using much simpler semi-empirical AM1 and CIS-AM1 calculations, and this observation supports usefulness of semi-empirical methods for quick exploratory calculations.

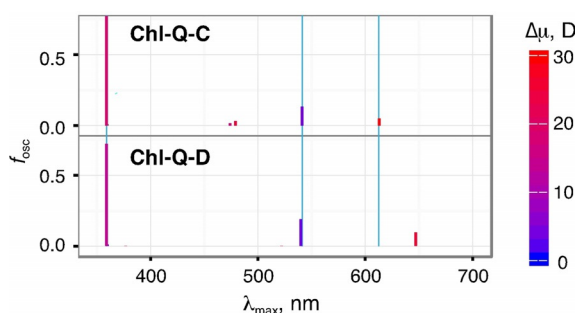


**Figure 7.** Calculated wavelengths, oscillator strengths, and associated differences in the dipole moments  $\Delta\mu = \mu(S_1) - \mu(S_0)$  ( $\Delta\mu$  shown using false color legend shown on the right side of the Figure) for the transitions from the ground to low-lying electronic states of Chl-Q-C (**8**) and Chl-Q-D (**5**) [B1LYP-40/6-31G(d) + PCM(toluene)].<sup>[63–67]</sup>

These experimental and computational results show that the CT state has lower energy than the LE state at the ground-state equilibrium geometry<sup>[69]</sup> thus indicating that PET in the dyads from Figure 1 corresponds to the Marcus inverted region (MIR). This result is further validated by the TD-DFT calculations used to find the equilibrium geometries for the first excited states. By assuming a quadratic form of the diabatic CT and LE states along the charge transfer reaction coordinate, we constructed the free energy profile of PET (Figure 8A) and fitted the  $\Delta G$  and  $\lambda$  values to be of  $\approx 0.55$  eV and  $\approx 0.31$  eV, respectively (see Figure S4 in the Supporting Information). The large positive difference between the free energy  $\Delta G$  and reorganization energy  $\lambda$  further supports the conjecture of the MIR regime for the PET in chlorin-quinone dyads.

The computational results presented above were obtained using the polarized continuum model with the parameters characteristic for toluene. The experimental results were also primarily obtained in toluene. As we see in Table S6 in the Supporting Information, in more polar solvent, that is, dichloromethane, the quantum yield of fluorescence is significantly dropped compared to toluene.

In the light of the finding that PET in chlorin-quinone dyads occurs in MIR, the observation of the reduced PET rate with increasing coupling is not surprising as it was theoretically predicted more than two decades ago.<sup>[70,71]</sup> In 1994, Stuchebrukhov and Song<sup>[70]</sup> applied the centroid coordinate method to the problem of electron transfer in MIR and demonstrated that the electron transfer rate must pass through the maximum and decrease exponentially with the increase of electronic coupling causing the splitting between the adiabatic levels to increase, as illustrated in Figure 8B. In 1996, Georgievskii et al.<sup>[71]</sup>

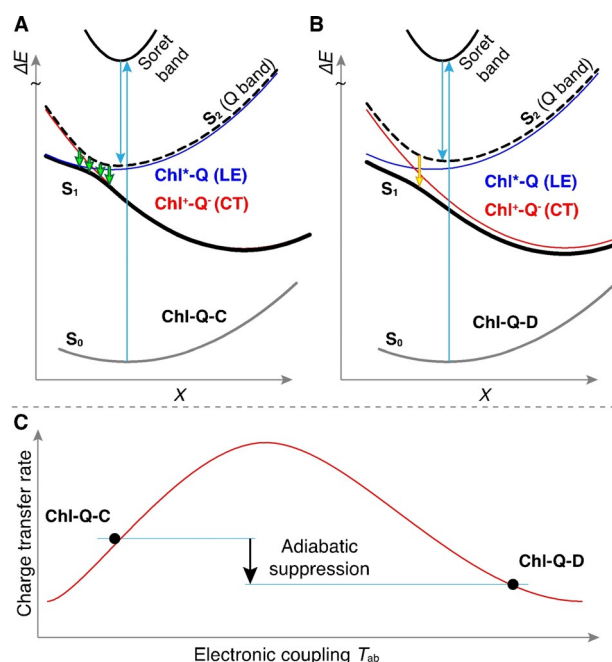


**Figure 8.** A,B) Schematic PET diagram for C and D isomers, respectively. Green arrows in panel A and yellow arrow in panel B highlight the adiabatic suppression of PET in Chl-Q-D (**5**). C) Schematic depiction of dependence of PET rate of electronic coupling in MIR.

applied Langevin equation to the same problem and arrived at the similar conclusion to dub the predicted effect as “adiabatic suppression”. Later theoretical works<sup>[72,73]</sup> also reproduced the effect of adiabatic suppression.

Despite the multiple theoretical predictions of the electron transfer suppression in the inverted region, to the best of our knowledge, there has been no experimental evidence for this effect in single-molecule donor-acceptor or donor-bridge-acceptor assemblies.<sup>[74]</sup> Accordingly, the current study of PET in chlorin-naphthoquinone dyads demonstrates for the first time an example of two assemblies with identical donor, acceptor, and bridge components, in which increased coupling leads to the decreased rate of PET due to the adiabatic suppression in MIR, as schematically depicted in Figure 8C.

## Conclusions

We have designed two simple donor-bridge-acceptor assemblies in which electronic coupling between donor and acceptor was varied by the orbital symmetry control while the charge transfer reorganization energy and exothermicity were kept constant. The photoinduced electron transfer in (Zn)Chl-Q dyads was shown to correspond to the inverted region of Marcus model, in which greater coupling led to the adiabatic suppression, that is, lower rate of charge transfer, due to the increased energy gap between the charge-transfer and locally excited states. Awareness of the fact that improved electronic coupling might lead to worse performance of the donor-acceptor or donor-bridge-acceptor assemblies is important for the design of molecules for photovoltaic applications as it indicates that electronic coupling must be fine-tuned rather than maximized in the donor-bridge-acceptor assemblies with large exothermicity of the charge transfer.

## Experimental Section

### Crystallographic data

Deposition numbers 2006646 and 2006647 (**17a** and **17b**) contain the supplementary crystallographic data for this paper. These data are provided free of charge by the joint Cambridge Crystallographic Data Centre and Fachinformationszentrum Karlsruhe Access Structures service [www.ccdc.cam.ac.uk/structures](http://www.ccdc.cam.ac.uk/structures).

## Acknowledgements

We thank Dr. P. Schulze, Mrs. I. Erxleben, Dipl.-Ing. J. Stelten (Institute of Organic and Analytical Chemistry, Laboratory Prof. Dr. D. Leibfritz, University of Bremen) for Mass spectrometry and NMR spectroscopy measurements, Dr. H.-M. Schiebel (TU Braunschweig) for interpretation of mass spectra and Dr. V. Azov for supporting manuscript preparation. We are indebted to Mrs. A. Lincke for performing analytical and preparative HPLC separations. This work was supported by Deutsche Forschungsgemeinschaft Mo 274/10 and the Extreme Science and Engineering Discovery Environment (XSEDE) TG-CHE170004. Open access funding enabled and organized by Projekt DEAL.

## Conflict of interest

The authors declare no conflict of interest.

**Keywords:** artificial photosynthesis · chlorin · electron transfer · quinone · symmetry

- [1] D. Gust, T. A. Moore in *Porphyrin Handbook, Vol. 8* (Eds.: R. Kadish, K. M. Smith, K. M. Guillard), Academic Press, San Diego, **2000**, pp. 153–190.
- [2] S. Fukuzumi in *Handbook of Porphyrin Science, Vol. 10* (Eds.: R. Kadish, K. M. Smith, K. M. Guillard), World Scientific, Singapore, **2010**, pp. 183–243.
- [3] D. M. Guldi, *Pure Appl. Chem.* **2003**, *75*, 1069–1075, and references therein.
- [4] F. D. Lewis, R. L. Letsinger, M. R. Wasielewski, *Acc. Chem. Res.* **2001**, *34*, 159–170.
- [5] W. R. Duncan, O. V. Prezhdo, *Annu. Rev. Phys. Chem.* **2007**, *58*, 143–184.
- [6] A. Mishra, M. K. R. Fischer, P. Bäuerle, *Angew. Chem. Int. Ed.* **2009**, *48*, 2474–2499; *Angew. Chem.* **2009**, *121*, 2510–2536.
- [7] M. V. Martínez-Díaz, G. de la Torre, T. Torres, *Chem. Commun.* **2010**, *46*, 7090.
- [8] J.-L. Wang, C. Wang, W. Lin, *ACS Catal.* **2012**, *2*, 2630–2640.
- [9] Y. Zhao, W. Liang, *Chem. Soc. Rev.* **2012**, *41*, 1075–1087.
- [10] F.-P. Montforts, I. Vlasiouk, S. Smirnov, M. Wedel, *J. Porphyrins Phthalocyanines* **2003**, *7*, 651–666.
- [11] S. Smirnov, I. Vlasiouk, O. Kutzki, M. Wedel, F.-P. Montforts, *J. Am. Chem. Soc.* **2002**, *124*, 4212–4213.
- [12] N. V. Tkachenko, A. Efimov, H. Lemmetyinen in *Handbook of Porphyrin Science, Vol. 42* (Ed.: R. Kadish, K. M. Smith, K. M. Guillard), World Scientific, Singapore, **2016**, pp. 121–171.
- [13] J. M. Warman, M. P. De Haas, J. W. Yerhoeven, M. N. Paddon-Row, *Adv. Chem. Phys.* **1999**, *106*, 571–601.
- [14] P. F. Barbara, T. J. Meyer, M. A. Ratner, *J. Phys. Chem.* **1996**, *100*, 13148–13168.
- [15] H. Kurreck, M. Huber, *Angew. Chem. Int. Ed. Engl.* **1995**, *34*, 849–866; *Angew. Chem.* **1995**, *107*, 929–947.
- [16] G. J. Kavarnos, *Fundamentals of Photoinduced Electron Transfer*, VCH, Weinheim, **1993**.
- [17] “Fundamental concepts of photoinduced electron transfer”: G. J. Kavarnos in *Photoinduced Electron Transfer I. Topics in Current Chemistry, Vol. 156* (Ed.: J. Mattay), Springer, Berlin, **1990**, pp. 21–58.
- [18] D. Gust, T. A. Moore, A. L. Moore, *Acc. Chem. Res.* **1993**, *26*, 198–205.
- [19] M. R. Wasielewski, *Chem. Rev.* **1992**, *92*, 435–461.
- [20] K. D. Jordan, M. N. Paddon-Row, *Chem. Rev.* **1992**, *92*, 395–410.
- [21] Y. Zeng, M. B. Zimmt, *J. Am. Chem. Soc.* **1991**, *113*, 5107–5109.
- [22] Y. Zeng, M. B. Zimmt, *J. Phys. Chem.* **1992**, *96*, 8395–8403.
- [23] M. B. Zimmt, *Chimia* **1997**, *51*, 82–89.
- [24] K. Wynne, S. M. LeCours, C. Galli, M. J. Therien, R. M. Hochstrasser, *J. Am. Chem. Soc.* **1995**, *117*, 3749–3753.
- [25] R. M. Williams, M. Koeberg, J. M. Lawson, Y.-Z. An, Y. Rubin, M. N. Paddon-Row, J. W. Verhoeven, *J. Org. Chem.* **1996**, *61*, 5055–5062.
- [26] Y. Sakata, H. Tsue, M. P. O’Neil, G. P. Wiederrecht, M. R. Wasielewski, *J. Am. Chem. Soc.* **1994**, *116*, 6904–6909.
- [27] A. Helms, D. Heiler, G. McLendon, *J. Am. Chem. Soc.* **1991**, *113*, 4325–4327.
- [28] K. K. Jensen, S. B. van Berlekom, J. Kajanus, J. Mårtensson, B. Albinsson, *J. Phys. Chem. A* **1997**, *101*, 2218–2220.
- [29] T. M. Figueira-Duarte, K. Müllen, *Chem. Rev.* **2011**, *111*, 7260–7314.
- [30] M. R. Talipov, T. S. Navale, R. Rathore, *Angew. Chem. Int. Ed.* **2015**, *54*, 14468–14472; *Angew. Chem.* **2015**, *127*, 14676–14680.
- [31] R. A. Marcus, *J. Chem. Phys.* **1956**, *24*, 966–978.
- [32] N. R. Kestner, J. Logan, J. Jortner, *J. Phys. Chem.* **1974**, *78*, 2148–2166.
- [33] P. Siders, R. A. Marcus, *J. Am. Chem. Soc.* **1981**, *103*, 741–747.
- [34] P. Siders, R. J. Cave, R. A. Marcus, *J. Chem. Phys.* **1984**, *81*, 5613–5624.
- [35] R. J. Cave, P. Siders, R. A. Marcus, *J. Phys. Chem.* **1986**, *90*, 1436–1444.
- [36] Z. S. Yoon, J. Yang, H. Yoo, S. Cho, D. Kim in *Handbook of Porphyrin Science, Vol. 1* (Eds.: R. Kadish, K. M. Smith, K. M. Guillard), World Scientific, Singapore, **2010**, pp. 439–505.

- [37] H. Tamiaki, M. Kunieda in *Handbook of Porphyrin Science, Vol. 11* (Eds.: R. Kadish, K. M. Smith, K. M. Guillard), World Scientific, Singapore, **2011**, pp. 223–290.
- [38] T. Nikkonen, M. M. Oliva, A. Kahnt, M. Muuronen, J. Helaja, D. M. Guldi, *Chem. Eur. J.* **2015**, *21*, 590–600.
- [39] S. Fukuzumi, K. Ohkubo, H. Imahori, J. Shao, Z. Ou, G. Zheng, Y. Chen, R. K. Pandey, M. Fujitsuka, O. Ito, K. M. Kadish, *J. Am. Chem. Soc.* **2001**, *123*, 10676–10683.
- [40] A. R. Holzwarth, M. Katterle, M. G. Müller, Y.-Z. Ma, V. Prokhorenko, *Pure Appl. Chem.* **2001**, *73*, 469–474.
- [41] J. Helaja, A. Y. Tauber, Y. Abel, N. V. Tkachenko, H. Lemmetyinen, I. Kilpeläinen, P. H. Hynninen, *J. Chem. Soc. Perkin Trans. 1* **1999**, 2403–2408.
- [42] N. V. Tkachenko, L. Rantala, A. Y. Tauber, J. Helaja, P. H. Hynninen, H. Lemmetyinen, *J. Am. Chem. Soc.* **1999**, *121*, 9378–9387.
- [43] M. R. Wasielewski, G. P. Wiederrecht, W. A. Svec, M. P. Niemczyk, *Sol. Energy Mater. Sol. Cells* **1995**, *38*, 127–134.
- [44] M. Gouterman in *Porphyryns, Vol. 3* (Ed.: D. Dolphin), Academic Press, New York, **1978**, pp. 1–165.
- [45] C. Weiss in *Porphyryns, Vol. 3* (Ed.: D. Dolphin), Academic Press, New York, **1978**, pp. 211–223.
- [46] A. Ghosh in *Porphyry Handbook, Vol. 7*, San Diego, **2000**, pp. 1–38.
- [47] M. J. Stillman in *Handbook of Porphyrin Science, Vol. 14* (Eds.: R. Kadish, K. M. Smith, K. M. Guillard), World Scientific, Singapore, **2011**, pp. 461–524.
- [48] M. Gouterman, *J. Chem. Phys.* **1959**, *30*, 1139–1161.
- [49] For a short paper related to this publication see: Y. Abel, F.-P. Montforts, *Tetrahedron Lett.* **1997**, *38*, 1745–1748.
- [50] F.-P. Montforts, *Angew. Chem. Int. Ed. Engl.* **1981**, *20*, 778–779; *Angew. Chem.* **1981**, *93*, 795–796.
- [51] F.-P. Montforts, U. M. Schwartz, *Liebigs Ann. Chem.* **1985**, *1985*, 1228–1253.
- [52] F.-P. Montforts, U. M. Schwartz, *Angew. Chem. Int. Ed. Engl.* **1985**, *24*, 775–776; *Angew. Chem.* **1985**, *97*, 767–768.
- [53] F.-P. Montforts, J. W. Bats, *Helv. Chim. Acta* **1987**, *70*, 402–411.
- [54] O. Kutzki, F.-P. Montforts, *Synlett* **2001**, *2001*, 0053–0056.
- [55] T. Könekamp, A. Ruiz, J. Duwenhorst, W. Schmidt, T. Borrmann, W.-D. Stohrer, F.-P. Montforts, *Chem. Eur. J.* **2007**, *13*, 6595–6604.
- [56] N. H. Vu, J.-E. Damke, T. Borrmann, L. Latos-Grażyński, F.-P. Montforts, *Helv. Chim. Acta* **2014**, *97*, 188–196.
- [57] G. Haake, D. Struve, F.-P. Montforts, *Tetrahedron Lett.* **1994**, *35*, 9703–9704.
- [58] Y. Abel, E. Haake, G. Haake, W. Schmidt, D. Struve, A. Walter, F.-P. Montforts, *Helv. Chim. Acta* **1998**, *81*, 1978–1996.
- [59] M. Roth, P. Dubs, E. Götschi, A. Eschenmoser, *Helv. Chim. Acta* **1971**, *54*, 710–734.
- [60] S. Ofner, V. Rasetti, B. Zehnder, A. Eschenmoser, *Helv. Chim. Acta* **1981**, *64*, 1431–1443.
- [61] F.-P. Montforts, M. Osmer, D. Leupold in *Handbook of Porphyrin Science, Vol. 25* (Eds.: R. Kadish, K. M. Smith, K. M. Guillard), World Scientific, Singapore, **2012**, pp. 265–307.
- [62] O. Kennard, *Supramolecular Chemistry* **1993**, *1*, 277–295.
- [63] M. Renz, K. Theilacker, C. Lambert, M. Kaupp, *J. Am. Chem. Soc.* **2009**, *131*, 16292–16302.
- [64] M. R. Talipov, A. Boddeda, Q. K. Timerghazin, R. Rathore, *J. Phys. Chem. C* **2014**, *118*, 21400–21408.
- [65] M. R. Talipov, R. Jasti, R. Rathore, *J. Am. Chem. Soc.* **2015**, *137*, 14999–15006.
- [66] M. R. Talipov, M. V. Ivanov, S. A. Reid, R. Rathore, *J. Phys. Chem. Lett.* **2016**, *7*, 2915–2920.
- [67] M. R. Talipov, T. S. Navale, M. M. Hossain, R. Shukla, M. V. Ivanov, R. Rathore, *Angew. Chem. Int. Ed.* **2017**, *56*, 266–269; *Angew. Chem.* **2017**, *129*, 272–275.
- [68] The assemblies with free-base chlorin moiety were computationally studied for the tautomeric form in which the inner nitrogen atoms from pyrroles B and D were protonated (as shown in Figure 1). This tautomeric form was by 18–40 kJ mol<sup>-1</sup> more stable than the form with the protonated nitrogen atoms from pyrroles A (saturated) and C (see Table S11 in the Supporting Information), in agreement with the previous NMR studies of tautomeric forms of chlorin-based compounds (Ref. [41]).
- [69] The equilibrium geometry of the ground state is almost identical to that of the LE-state, as evidenced by the low values of the Stokes shift (Table S6 in the Supporting Information) and TD-DFT geometry optimizations (Tables S12 and S13 in the Supporting Information).
- [70] A. A. Stuchebrukhov, X. Song, *J. Chem. Phys.* **1994**, *101*, 9354–9365.
- [71] Y. Georgievskii, A. I. Burshtein, B. M. Chernobrod, *J. Chem. Phys.* **1996**, *105*, 3108–3120.
- [72] A. I. Burshtein, V. Gladkikh, *Chem. Phys.* **2006**, *325*, 359–364.
- [73] Y. Zhao, M. Han, W. Liang, H. Nakamura, *J. Phys. Chem. A* **2007**, *111*, 2047–2053.
- [74] a) A. L. Thompson, T.-S. Ahn, K. R. J. Thomas, S. Thayumanavan, T. J. Martínez, C. J. Bardeen, *J. Am. Chem. Soc.* **2005**, *127*, 16348–16349 showed a somewhat similar effect in carbazole(D)–naphthalimide(A) assemblies with two different bridges, that is, *meta*- and *para*-phenylacetylene. Later a theoretical report, b) M. H. Lee, B. D. Dunietz, E. Geva, *J. Phys. Chem. C* **2013**, *117*, 23391–23401, showed that both assemblies correspond to MIR. However, it is unclear whether the observed suppression of PET arises due to the specific effects of different bridges, as was suggested in the original report, or to the effect of MIR.

Manuscript received: June 5, 2020

Accepted manuscript online: July 6, 2020

Version of record online: November 19, 2020